

Structures of solid hydrogen at 300K

Graeme J. Ackland¹ and John S. Loveday*

¹Centre for Science at Extreme Conditions and School of Physics and Astronomy, University of Edinburgh, Edinburgh, U.K.

(Dated: March 4, 2022)

We present results predicting experimentally measurable structural quantities from molecular dynamics studies of hydrogen. In doing this, we propose a paradigm shift for experimentalists – that the predictions from such calculations should be seen as the most likely hypotheses. Specifically, the experimental results should be aiming to distinguish between the candidate low-energy structures, rather than aiming to solve the simplest structure consistent with the data. We show that the room temperature X-ray diffraction patterns for hydrogen phases I, III, IV and V are very similar, with only small peaks denoting symmetry-breaking from the hcp Phase I. Because they incorporate atomic displacements the XRD patterns implied by molecular dynamics calculations are very different from those arising from the static minimum enthalpy structures found by structure searching. Simulations also show that within Phase I the molecular becomes increasingly confined to the basal plane and suggest the possibility of an unusual critical point terminating the Phase I-III boundary line.

Solid hydrogen has proved to be one of the most challenging topics in high-pressure physics, both theoretically and experimentally. At room temperature, information about the crystal structure is available largely through indirect methods such as spectroscopy^{1–8}. With the exception of two neutron diffraction studies^{9,10} at ~ 30 GPa, structural studies are confined to X-ray studies^{11–14} which are largely insensitive to molecular orientation. To exploit these studies fully, it is important to have models for the crystal structure. In recent years, *ab-initio* structure-search methods have been highly successful at determining the possible classical ground state structures^{15–19}. These have shown a panoply of possible phases, typically with large unit cells and low symmetry, often very close in energy.

The calculations have an unquantifiable uncertainty associated with the choice of functional^{20–23}. Furthermore, the effects of quantum nuclear-motion are significant, with zero-point energy being much larger than typical energy differences between structures. So despite all this work, no consensus has emerged for the crystal structure of any high pressure phase. Nevertheless, some patterns have emerged which suggest the calculated structures are consistent with the major experimental findings²⁴.

Since the discovery of a Raman-active phonon, Phase I of hydrogen has been accepted as a hexagonal close-packed (hcp) structure of rotating molecules. On cooling at pressure, a transformation occurs to a “broken symmetry” Phase II, characterised by a discontinuous change in H₂ vibron frequency and the appearance of several low-frequency modes. This transition occurs at temperatures and densities where quadrupole interactions become significant, and these are likely to be the driving force. The I-II transformation has no distinctive signature in X-ray diffraction¹², suggesting that it is an orientational ordering of the hydrogen molecules on the hcp lattice. Many of the most stable candidate structures from density functional theory (DFT) calculation are in this category.^{15,25}

At higher pressures, above 160 GPa at low-T, pronounced weakening in vibron frequency and further

changes in the low frequency spectra heralds Phase III. It is debatable whether there is any signature of this phase in X-ray diffraction: at most it is a small distortion or modulation of the hcp structure. Perhaps the most distinctive signature of Phase III is the sudden appearance of a strong infrared signal, indicating that the structure has broken inversion symmetry. At still higher pressures, darkening of the samples suggests a bandgap closure in a molecular phase, and reflectivity reveals a transition to a metallic phase, predicted by DFT to be initially molecular then a low-coordinated atomic solid. Ultimately, hydrogen will metallize and the molecular bonds will break, though it is unclear whether these processes are simultaneous^{26,27}.

At room temperature, the Phase I transforms first to phase III at around 180 GPa, then to a Phase IV at around 230 GPa which has not been observed at low temperature. Phase IV is characterized by the appearance of a second, (and possibly third) high frequency vibron^{5,28–30}. Under further pressurization, the two vibrons remain and changes in the low frequency Raman spectra may indicate transformations to further phases IV' and V. It is assumed that metallization will occur, but this has not been observed at room temperature.

We have spent several years making comparisons between DFT data and the spectroscopic data, using lattice dynamics and molecular dynamics, including path integral methods^{24,31–37}. We have used different exchange-correlation functionals and different treatments of anharmonicity, and our conclusion is that these methods are not sufficiently accurate to obtain quantitative agreement for transition pressures or vibrational frequencies. Nevertheless, in this paper we will present some predictions about crystal structures which are experimentally measurable.

A. *ab initio* molecular dynamics

Structure search algorithms work well for low temperature phases with harmonic phonons, but even at room

temperature hydrogen is far from harmonic. Ab initio molecular dynamics (AIMD) is able to probe this region. Limitations on timescales and system sizes mean that accurate free energy calculations are impossible, however, just as with structure search, AIMD can reveal symmetry and structure of *candidate* phases.

Most previous AIMD was done with the PBE functional³⁸. However, it is now becoming obvious that this *de facto* standard functional has a specific failing: it overstabilizes metallic structures relative to molecular ones. This can be traced to a design feature - PBE does not reproduce the energy in the limit of large $\nabla \ln(\rho)$. This does not usually cause problems: when studying metallic phases, the high $\nabla \ln(\rho)$ regime is not sampled, and in comparing molecular phases the error cancels out. It is only in the specific case of a molecule-metal transition that it becomes critical. In this work we also use the BLYP functional^{39,40} which, though simple, does capture the high $\nabla \ln(\rho)$ limit and gives a better description of H₂ molecular dissociation.

1. Phases

Experimentally, four numbered phases have been reported based on spectroscopy. In addition, two “primed” sub-phases have been identified, giving a sequence I-I’-III-IV-IV’-V. The broken symmetry phase II and metallic phases have been observed only at low temperatures.

Previous MD on phases of hydrogen at 300K suggests only Phase III involves harmonic (or even anharmonic) oscillations about well-defined atomic positions: all other phases have molecular rotation, reorientation and at higher pressures significant rebonding. All of them can be characterised by molecular “motifs” located on “hexagonal close packed” lattice sites. This underlying P6₃/mmc space group provides the highest possible symmetry - changes to the motifs lower this symmetry.

Surprisingly, previous calculations were done in the NVT ensemble, so that the crystallographic measurable, the c/a ratio, has not previously been calculated. For close-packing of hard spheres, the c/a ratio is $\sqrt{8/3} = 1.633$. Cohesion in solid hydrogen arises primarily from van der Waals forces which drop off as $1/r^6$. The Lennard-Jones potential captures this behavior, and stabilizes the hcp structure with $\sqrt{8/3} \simeq 1.633$.⁴¹

B. AIMD runs

We ran a large number of molecular dynamics calculations to evaluate the various structures. The same sequence of phases are observed independent of exchange-correlation functional. Compared with PBE, the BLYP functional gives systematically higher pressures at a given density (Fig.3). It also makes better defined hydrogen molecules with higher vibrational frequencies.

Calculations were initiated from different candidate structures identified from previous *Ab-Initio* Random Structure Search, AIRSS, calculations for phase II, III and IV candidates^{15,16}. None of those low-symmetry structures remained stable at 300K, all transformed to higher symmetry structures. Nevertheless, based on average molecular positions some distinct structures were observed which can be assigned to non-metallic phases I, III, IV, V plus a molecular metallic phase *Cmca* and atomic metal *I4amd*.

1. Finite Size Effects

The complexity of phases III, IV and V mean that they are extremely sensitive to finite size effects. As shown in Table I, only phases compatible with the initial conditions are observed. e.g. the $BG'BG''$ phase IV candidate is hexagonal a four layer repeat with six atoms per layer - self evidently, only super-cells with multiples of 24 atoms can find this structure, while the $BG'_xBG'_yBG'_z$ candidate requires a multiple of six hexagonal layers.

Furthermore, there is a probability of finding a layer with incorrect stacking. This is of order $\exp(-N\Delta F/kT)$, where ΔE is the excess free energy per atom in the mis-stacked layer and N the number of atoms per layer. Evidently, this goes to zero at large N - *mis-stackings never occur in thermodynamic equilibrium*. However, in finite systems it may happen: with 12 atoms per layer, even fluctuations between B and G occur. We found that with less than 54 atoms *per layer* spurious fluctuations between types of G layer at the size of the system do still occur, which gives a spuriously high mean-squared displacement.

For a simulation to even have the *possibility* of correctly describing Phase IV, it should accommodate both $BG'BG''$ and $BG'_xBG'_yBG'_z$ candidates, and have layers containing a multiple of 6 atoms. To also prevent spurious fluctuations required a minimum of 648 atom (i.e. 54 atoms per layer). This cell size was used in the region of the phase transition.

Finite size effects are generally regarded as a problem, but if properly understood they can be turned to advantage. Specifically, by adjusting the cell size to be incompatible with the stable phase, we can probe metastable phases. This enables us to predict experimental signatures for all candidate phases, and thus determine whether they could be distinguished by diffraction or spectroscopy.

All the cells considered can transform into Phase I, which allows us to determine whether the transitions are first order. We monitor three order parameters, the density, the c/a ratio and the angle between the molecules and the c -axis.

At the lowest pressures Phase I comprises freely rotating H₂ molecules. Fig.2 shows that, as expected, at low pressures c/a tends to the ideal ratio but gets smaller under pressure. To understand why this might be, we

examined the cosine of θ between the molecular axis and the c -axis (Fig.4). For a free rotor, this would average 0.5. This is the case at low pressure, but even within Phase I, as the pressure increases, the molecule increasingly rotates in the plane. This reduction of c/a has been observed by X-ray diffraction^{12,13} at low temperature, and can now confidently be ascribed to the molecule changing from spherical to toroidal. The torus is still compatible with the $P6_3/mmc$, so this symmetry breaking of the molecule does not require a structural phase transition.

This change from spherical to torus rotation is not observed in NVT ensemble simulations with ideal c/a , emphasizing the importance of choice of ensemble.

At higher pressures there is a transformation to Phase III. Structure searching has revealed a number of candidate structures which were initially described by reference to the nuclear positions as different stackings of “distorted Graphite-like layers”. However, considering the molecular (rather than atomic) positions reveals that this is just an hcp lattice with the minimum of broken symmetry required for molecular orientation (Fig.1(a)). The molecular dynamics shows a similar orientational order (see Fig.1b).

To understand the highest pressure structures, fig. 5 relate the observed structures to the simple MgB_2 structure with a hydrogen molecule on the Mg site (a triangular “B” layer) and hydrogen atoms on the boron sites (a graphitic layer “G”). This structure has alternating layers, so the c -glide symmetry is broken and the space group becomes $P6/mmm$. In the molecular dynamics, this MgB_2 structure is recognised *on average* at very high pressures. However it is energetically highly unstable to formation of molecules: the trajectories cannot be described in terms of harmonic oscillations: the boron lattice site is not a local maximum of energy.

The structures observed for phases IV, IV' and V are described in terms of symmetry-breaking from MgB_2 so as to form molecules in the layers. There are multiple ways of doing this (Figure 5). The molecules in these layers tend to remain in plane, meaning that the c/a ratio falls further.

In figure 1 we show a schematic of how a layer in Phase III emerges from Phase I. The large circles represent molecular locations on a perfect close packed plane. We observe that the molecules in Phase I come to lie in the plane at high pressure. Now, assume that each in-plane molecule points towards a gap between neighbours and is not aligned with its neighbours. These two rules are sufficient to uniquely define all the molecule orientations, as shown by the arrows. Figure 1 also shows a picosecond time-average from 648-atom BLYP simulation at 180GPa, assigned Phase III. Although the non-centrosymmetric motif is clear, there are frequent local rotations and reorientations.

This ordering leads to a 3-molecule repeating cell, and spontaneously breaks inversion symmetry. This broken symmetry means that the molecule moves off the hcp site

and acquires a dipole moment. This dipole moment is responsible for the strong IR signal which is a key signature of Phase III. The movement off-site might be detectable by X-ray scattering, but new peaks associated with it are weak, and it only induces a small change in relative intensity of the three main peaks compared with hcp.

Furthermore, there are two non-equivalent sites for the next layer (2/3rds unmarked, 1/3rd red circles). Consequently, a 3D unit cell must be based on (at least) two of these 3-molecule 2D layered cell. The lowest energy structures identified by *ab initio* structure search for Phase III, $C2/c - 24$ and $P6_122$, involve a 4 and 6 layer repeat of this layer.

Determination of the high temperature structures was done by layer-by layer *ab oculo* analysis using vmd. In addition to snapshots or movies proved, two analyses proved extremely useful.

- Plots of time-averaged atomic positions. The B -layers image as a triangular lattice with two atoms coincident at each lattice site. The G'' layers image as a large triangular lattice with six atoms coincident at each site. The G' layers typically image as separate atoms, similar to a snapshot, although after many picosecond the pattern is destroyed by diffusion within this layer.
- Dot-plots for all atoms, at all times. The B -layers image as spheres or small donuts, the G'' layers image as triple-arcs or large donuts, with some evidence of six- and three-fold rotational symmetry, the G' layers image as separate atoms.

We carried out limited path Integral molecular dynamics, which show relatively little qualitative change from the classical picture, the main effect being a wider variation in molecular length due to zero-point energy. There is some small effect on the phase boundaries.

2. Simulated Crystallography

We have calculated the diffraction pattern from the positions of the atoms from a sample of MD runs. in phases I, III, IV and V. This was done by combining the positions from the final 2ps of the MD trajectory and treating the supercell as a single cell with P1 symmetry. The resulting assemblage of approximately 50000 atomic positions thus models not only the average positions of the atoms within the structure but also the atomic displacements, including anisotropy and anharmonicity, about these average positions. The calculations were done using the GSAS-II program⁴² and assumed a standard hydrogen form factor and an X-ray wavelength of 0.7 Å.

Figure 6 shows that at 140GPa, the XRD patterns for two lowest energy candidate structures for Phase II $P6_3/m$ and $Pca2_1$ are similar, the distinguishing feature being a small peak splitting in $Pca2_1$ or small additional

peaks in $P6_3/m$. XRD of either supercell gives 3 significant diffraction peaks, which can readily be indexed as (100) (002) and 101) from an hcp structure. In the 300K MD, simulations started in either structure transform to an identical hindered-rotor hcp Phase I.

Phase III is stable at 190GPa, and Fig.7 shows that again the two zero-temperature candidate structures $P6_122$ and $B2/n$ (sometimes called by its alternative setting $C2/c$) have similar 2-peak patterns, being distinguished only by weak reflections. In the MD, the two-peak pattern persists, but unusually as the temperature increases, a third small peak grows in prominence, while other small peaks vanish. On simulated cooling, the XRD pattern transforms continuously from being characteristic of phase I, to characteristic of Phase III, which is consistent with the gradual onset of short ranged orientational order.

There are several candidates for Phase IV, which can be simulated separately by making supercells incompatible with the other. Fig.8 shows the calculated diffraction pattern from two of them, and again the two candidate give near identical patterns with a very close doublet and a third peak at lower angle. Ignoring the small peaks, would be possible to index these peaks to hcp, with an anomalously small c/a ratio as shown in Fig.2. Fig.8 also shows that a very strong additional peak appears with the Ibam structure which corresponds to symmetric graphitic layers, a candidate for Phase V which is stable in MD above 400GPa^{31,43}. This is perhaps the first phase which can be easily distinguished from hcp with XRD data.

The original 1935 prediction of metallic hydrogen by Wigner and Huntington⁴⁴ is based on free electron theory, and analysis of metallic hydrogen is still based on this premise⁴⁵. Since hydrogen has no core electrons, a free-electron phase of solid hydrogen would have a featureless X-ray diffraction pattern. However, calculations using DFT show that the electrons are still well localized, and X-ray diffraction from metallic hydrogen will be nearly as strong as from molecular phases⁴⁷.

Very recently, a report of the experiments simulated in this work has appeared⁴⁶. In this paper, the sharp turn of the c/a ratio at the transition from Phase I - IV at around 200GPa is observed. This is the signature of the phase transformation from hcp to a multilayer hexagonal structure, with the appearance of a second vibron. The experiment rules out any of the lower symmetry zero-

temperature structures found from structure searching as being candidates for Phase IV.

Ji *et al* attribute their results to a $P6_3/mmc$ structure. This would be a unique example of an isostructural electronic transition between two non-metallic phases. We have reproduced the band structure and recalculated this structure using BLYP, find it to be energetically unstable at all pressures, as it is with PBE. The associated variation in c/a is shown in Fig. ?? and diffraction pattern in Fig.7, both are in qualitative disagreement with Ji *et al*'s own XRD data: in particular the c/a ratio of the proposed structure *increases* with pressure, whereas the XRD indicates a decrease. Furthermore, the $P6_3/mmc$ structure is unstable in MD, transforming spontaneously to the normal Phase I, or lower symmetry III and IV structures previously identified.

C. Discussion and Conclusions

We have carried out extensive molecular dynamics simulations of high pressure hydrogen at room temperature using two different exchange correlation functionals. The functionals give the same sequence of phases, but with a difference of 20-30GPa in pressure. The sequence of phases, I-III-IV-V is in accordance with experiment, with the pressure calculated using in BLYP closer agreement. Molecular rotation (or disorder) increases the symmetry so that the calculated diffraction pattern for Phases III and IV is much more similar to Phase I than to their zero-temperature relaxed structures previously taken as exemplars.

Under pressure the free rotors of Phase I become more and more inhibited, with the molecules preferentially rotating in-plane. This loss of sphericity causes a drop in the c/a ratio away from ideal. In phase III, the rotation stops and the molecules lie in plane, however the diffraction pattern structure is still close to hcp with a still-lower c/a ratio. A 3% drop in the c/a ratio and change in its pressure-slope accompanies the transformation.

Our simulated XRD patterns, and the implied variation in the c/a ratio, are in excellent agreement with recent XRD data. The room temperature, high pressure phases of hydrogen can therefore confidently be ascribed to hexagonal structures with inhibited rotors, up to at least 250GPa.

GJA acknowledges the support of the European Research Council Grant Hecate Reference No. 695527

* g.j.ackland@ed.ac.uk

¹ A. F. Goncharov, R. J. Hemley, H.-K. Mao, and J. Shu, Phys.Rev.Letters **80**, 101 (1998).

² A. F. Goncharov, E. Gregoryanz, R. J. Hemley, and H.-K. Mao, Proceedings of the National Academy of Sciences **98**, 14234 (2001).

³ P. Loubeyre, F. Occelli, and R. LeToullec, Nature **416**, 613 (2002).

⁴ P. Dalladay-Simpson, R. T. Howie, and E. Gregoryanz, Nature **529**, 63 (2016).

⁵ R. T. Howie, C. L. Guillaume, T. Scheler, A. F. Goncharov, and E. Gregoryanz, Phys. Rev. Letters **108**, 125501 (2012).

⁶ C. S. Zha, Z. Liu, and R. J. Hemley, Phys. Rev. Letters **108**, 146402 (2012).

⁷ R. T. Howie, P. Dalladay-Simpson, and E. Gregoryanz, Nature materials **14**, 495 (2015).

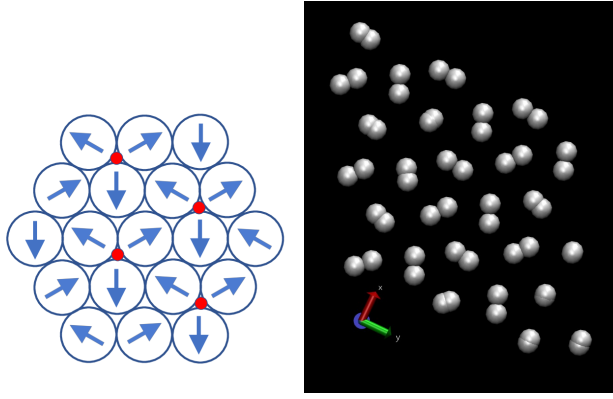


FIG. 1: Single G layer, All structures comprising stacking of these layers are labelled “Phase III”. (left) schematic: red dots show position of the 3-fold rotation axis. Blue arrows represent molecular axis. The orientation within the plane does not require any symmetry-breaking, however any orientation of molecules in planes above and below will break the symmetry and induce a dipole, as indicated by the direction the arrow. (right) time-averaged positions of atoms over 1ps from one layer in the 180GPa simulation using BLYP. All molecules are in-plane, apparently short bonds occur when the molecule has rotated through 180 degrees at some stage. Notice how molecules are displaced.

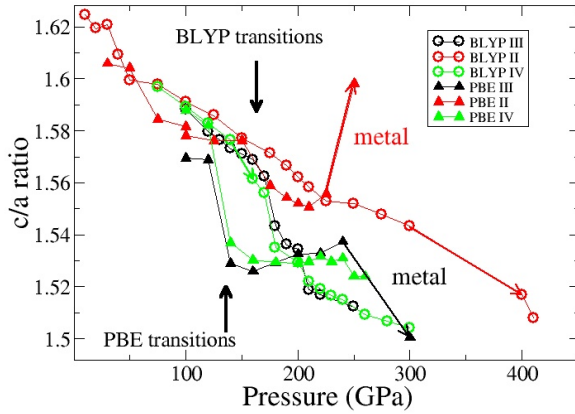


FIG. 2: Plot of c/a ratio for simulations in various cells. Arrows show sharp change in c/a with transition to phase IV, and more gradual change approaching phase III. Note the significant functional dependence in the calculated transition pressure. The very high pressure metallic $Cmca$ structures are twinned, so the change in “ c/a ratio” for the cell signifies the transition, but is not the c/a ratio of $Cmca$.

- ⁸ E. Gregoryanz, A. F. Goncharov, K. Matsuishi, H.-K. Mao, and R. J. Hemley, *Phys.Rev.Letters* **90**, 175701 (2003).
⁹ V. Glazkov, S. Besedin, I. Goncharenko, A. Irodova, I. Makarenko, V. Somenkov, S. Stishov, and S. Shilshtein, *JETP Letters* **47**, 763 (1988), ISSN 0021-3640.
¹⁰ I. Goncharenko and P. Loubeyre, *Nature* **435**, 1206 (2005).

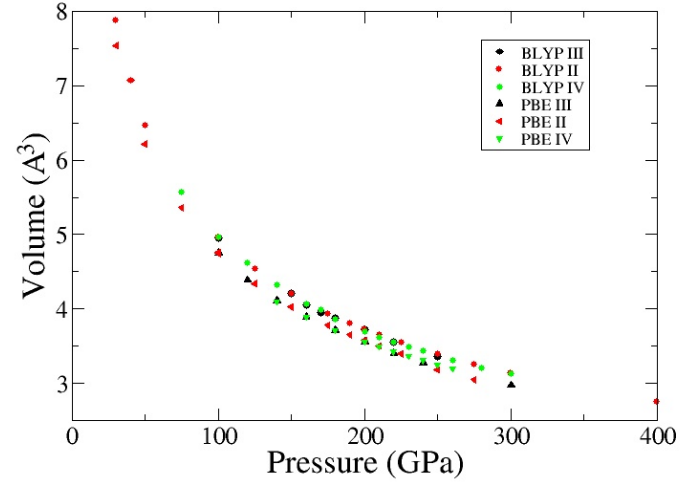


FIG. 3: Equation of state (volume per atom) for all structures with BLYP (circles) and PBE (triangles) showing that functional effects are much larger than structural differences, and the uncertainty due to functional is about 20GPa.

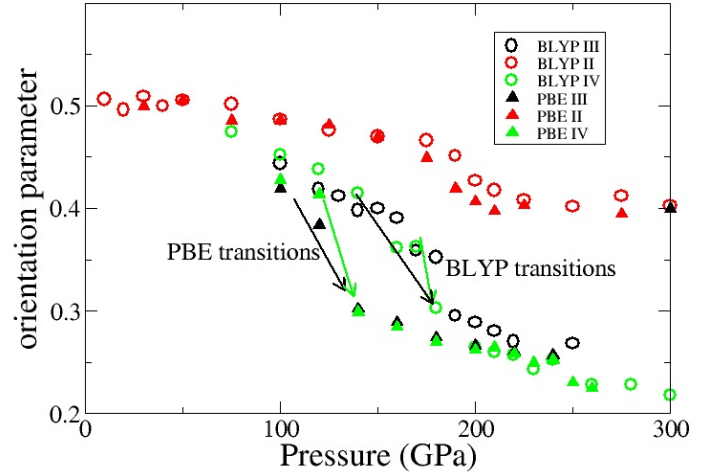


FIG. 4: Variation of angular orientation order parameter $\langle \cos \theta \rangle$ with pressure.

- ¹¹ R. Hemley, H. Mao, L. Finger, A. Jephcoat, R. Hazen, and C. Zha, *Physical Review B* **42**, 6458 (1990).
¹² P. Loubeyre, R. LeToullec, D. Hausermann, M. Hanfland, R. Hemley, H. Mao, and L. Finger, *Nature* **383**, 702 (1996).
¹³ Y. Akahama, M. Nishimura, H. Kawamura, N. Hirao, Y. Ohishi, and K. Takemura, *Phys. Rev. B* **82**, 060101 (2010).
¹⁴ Y. Akahama, H. Kawamura, N. Hirao, Y. Ohishi, and K. Takemura, in *Journal of Physics: Conference Series* (IOP Publishing, 2010), vol. 215, p. 012056.

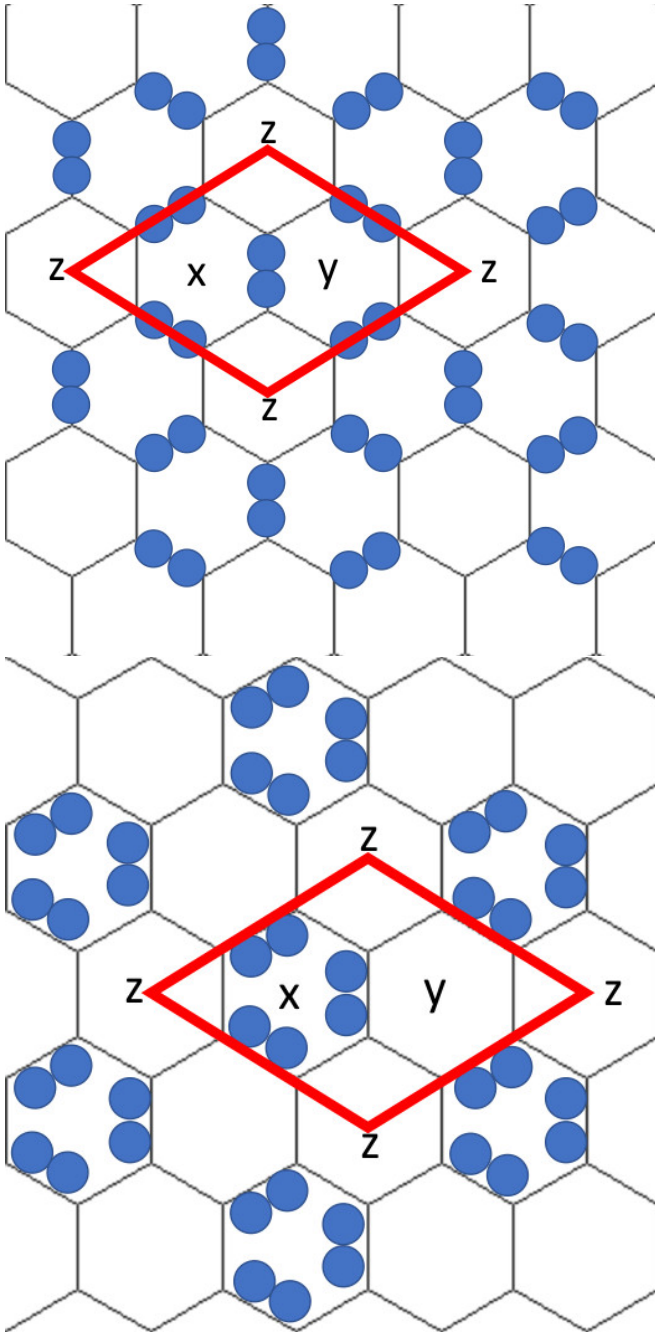


FIG. 5: Schematic of typical in-plane atomic positions in the so-called “graphitic” (G) layers of Phase IV. The red diamond shows a and b vectors for single unit cell. Each unit cell has two equivalent and one non-equivalent hexagon: x , y and z are used to label the layer stacking of the non-equivalent site. In this notation (a) G'_z , (b) G''_x . The molecular “B”-layers are like Phase-I and are not shown, they simply comprise a molecule at the center of each hexagon, again six atoms per layer. In static relaxation these B-molecules have well defined orientation (e.g. the Pbcn structure), but at room temperature they are disordered and re-orient on a 100fs timescale. Due to constraints from periodic boundary conditions, in MD simulation a two-layer cell in Phase IV PT conditions adopts BG'_z stacking, four layers $BG'_zBG''_z$, six layers $BG'_xBG'_yBG'_z$, eight layers $BG'_zBG''_zBG'_zBG''_z$.

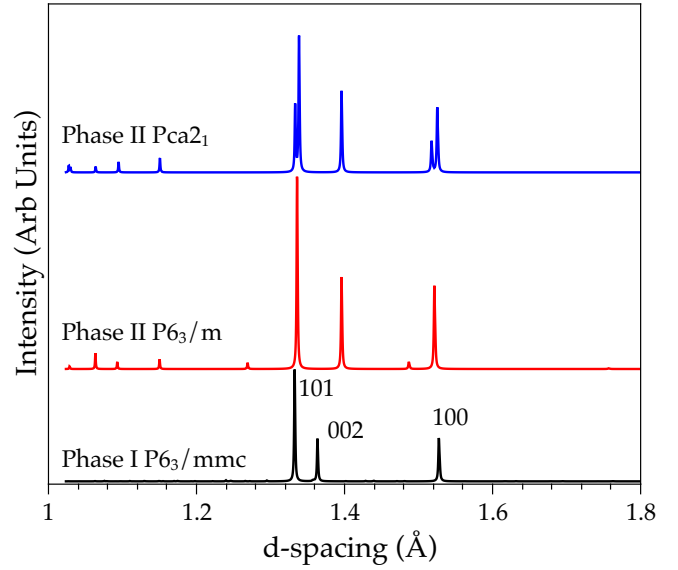


FIG. 6: Simulated X-ray diffraction patterns for Hydrogen Phase II at 140GPa. $P6_3/m$ and $Pca2_1$ are the zero-temperature ground states proposed by structure search. MD averaged over 2ps starting from $P6_3/m$ at 300K temperature is shown. Simulations starting from $Pca2_1$ or $P6_3/mmc$ are indistinguishable - all are Phase I.

- ¹⁵ C. J. Pickard and R. J. Needs, Nature Physics **3**, 473 (2007).
- ¹⁶ C. J. Pickard and R. J. Needs, Physica Status Solidi (b) **246**, 536 (2009).
- ¹⁷ C. J. Pickard, M. Martinez-Canales, and R. J. Needs, Phys. Rev. B **85**, 214114 (2012).
- ¹⁸ X.-Z. Li, B. Walker, M. I. Probert, C. J. Pickard, R. J. Needs, and A. Michaelides, Journal of Physics: Condensed Matter **25**, 085402 (2013).
- ¹⁹ B. Monserrat, R. J. Needs, E. Gregoryanz, and C. J. Pickard, Physical Review B **94**, 134101 (2016).
- ²⁰ S. Azadi and W. M. C. Foulkes, Phys. Rev. B **88**, 014115 (2013).
- ²¹ R. C. Clay III, J. Mcminis, J. M. McMahon, C. Pierleoni, D. M. Ceperley, and M. A. Morales, Phys. Rev. B **89**, 184106 (2014).
- ²² N. D. Drummond, B. Monserrat, J. H. Lloyd-Williams, P. L. Ríos, C. J. Pickard, and R. J. Needs, Nature communications **6** (2015).
- ²³ S. Azadi and G. J. Ackland, Physical Chemistry Chemical Physics **19**, 21829 (2017).
- ²⁴ I. B. Magdău, M. Marques, B. Borgulya, and G. J. Ackland, Phys.Rev.B **95**, 094107 (2017).
- ²⁵ H. Y. Geng, H. X. Song, J. Li, and Q. Wu, Journal of Applied Physics **111**, 063510 (2012).
- ²⁶ B. Holst, R. Redmer, and M. P. Desjarlais, Physical Review B **77**, 184201 (2008).
- ²⁷ W. Lorenzen, B. Holst, and R. Redmer, Phys. Rev. B **82**, 195107 (2010).
- ²⁸ R. T. Howie, T. Scheler, C. L. Guillaume, and E. Gregoryanz, Phys. Rev. B **86**, 214104 (2012).
- ²⁹ C. S. Zha, Z. Liu, M. Ahart, R. Boehler, and R. J. Hemley, Phys.Rev.Letters **110**, 217402 (2013).

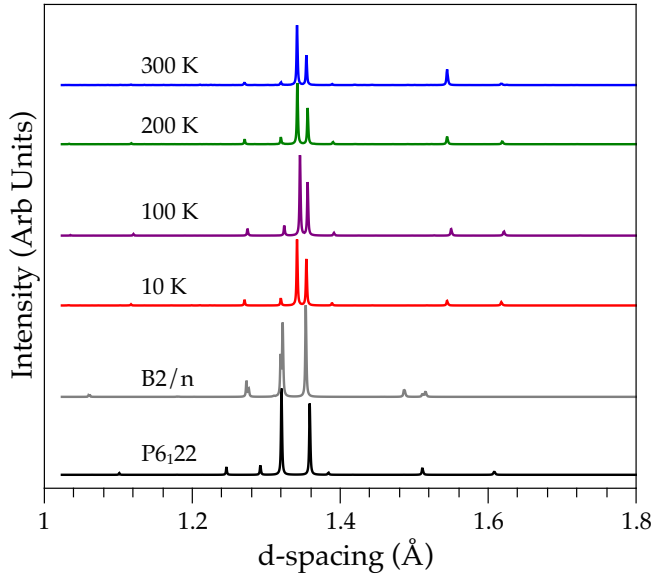


FIG. 7: Simulated X-ray diffraction patterns for Hydrogen Phase III at 190 GPa calculated using BLYP. B2/ n and P6₁22 are the zero-temperature ground states proposed by Pickard¹⁵ and by Monserrat¹⁹ respectively. MD is averaged over 2ps starting from P6₁22 at various temperatures.

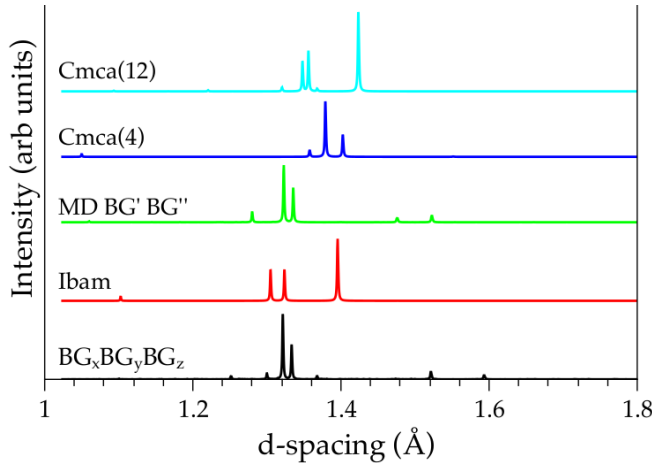


FIG. 8: Simulated X-ray diffraction patterns for Hydrogen Phase IV at 220 GPa. Ibam Pc and Pbcn are the zero-temperature ground states proposed by Pickard. MD for the two different hexagonal candidates (Fig. 5), is averaged over 2ps at 300K starting from Pbcn ($BG'BG''$) and starting from P6₁22 ($BG_xBG_yBG_z$).

- (2014).
- ³⁵ G. J. Ackland and I. B. Magdău, High Pressure Research **34**, 198 (2014).
 - ³⁶ I. B. Magdău, F. Balm, and G. J. Ackland, Journal of Physics: Conference Series **950**, 042059 (2017).
 - ³⁷ I. B. Magdău and G. J. Ackland, Phys. Rev. Lett. **118**, 145701 (2017).
 - ³⁸ J. P. Perdew, K. Burke, and M. Ernzerhof, Phys.Rev.Letters **77**, 3865 (1996).
 - ³⁹ C. Lee, W. Yang, and R. G. Parr, Physical review B **37**, 785 (1988).
 - ⁴⁰ A. D. Becke, Physical review A **38**, 3098 (1988).
 - ⁴¹ C. H. Loach and G. J. Ackland, Physical review letters **119**, 205701 (2017).
 - ⁴² B. H. Toby and R. B. von Dreele, Journal of Applied Crystallography **46**, 544 (2013).
 - ⁴³ I. B. Magdău, B. Tyson, B. Borgulya, and G. J. Ackland, writing (2016).
 - ⁴⁴ E. Wigner and H. Huntington, J. Chem. Physics **3**, 764 (1935).
 - ⁴⁵ R. P. Dias, O. Noked, and I. F. Silvera, Phys.Rev.Letters **116**, 145501 (2016).
 - ⁴⁶ C. Ji, B. Li, W. Liu, J. S. Smith, A. Majumdar, W. Luo, R. Ahuja, J. Shu, J. Wang, S. Sinogeikin, et al., Nature **573**, 558 (2019).
 - ⁴⁷ Ingo Loa, private communication

- ³⁰ P. Loubeyre, F. Occelli, and P. Dumas, Phys. Rev. B **87**, 134101 (2013).
- ³¹ I. B. Magdău and G. J. Ackland, Phys. Rev. B **87**, 174110 (2013).
- ³² I. Magdău and G. J. Ackland, **500**, 032012 (2014).
- ³³ G. J. Ackland and I. B. Magdău, Cogent Physics **2**, 1049477 (2015).
- ³⁴ R. T. Howie, I. B. Magdău, A. F. Goncharov, G. J. Ackland, and E. Gregoryanz, Phys. Rev. Letters **113**, 175501

Appendix

BLYP					
Pressure	Volume	c/a	$\langle \cos\theta \rangle$	initiated	Phase
10	11.9804	1.6247	0.506480	P63m	I
20	9.1007	1.619415	0.4962698	P63m	I
30	7.8787	1.620801	0.508926	P63m	I
40	7.0702	1.609334	0.4996069	P63m	I
50	6.4600	1.599574	0.5051744	P63m	I
75	5.5644	1.597964	0.5018897	P63m	I
100	4.9660	1.591320	0.4865163	P63m	I
125	4.5356	1.585926	0.4764345	P63m	I
150	4.2018	1.577247	0.4698209	P63m	I
175	3.9393	1.571384	0.4662826	P63m	I
190	3.8078	1.566554	0.4507833	P63m	I
200	3.7320	1.562305	0.4266832	P63m	I
210	3.6532	1.558341	0.4177813	P63m	I
225	3.5491	1.553017	0.4081023	P63m	I
250	3.3899	1.552009	0.4016243	P63m	I
275	3.2574	1.547899	0.41143	P63m	I
300	3.1358	1.54326	0.4024638	P63m	I
400	2.7490	1.517	0.3613476	P63m	Cmca
410	2.6943	1.508	0.442654	P63m	Cmca
100	4.9604	1.5883	0.4439265	P ₆₁ 22	I
120	4.6034	1.579752	0.4185463	P ₆₁ 22	I
130	4.4539	1.576561	0.4116525	P ₆₁ 22	I
140	4.3176	1.573193	0.397990	P ₆₁ 22	I
150	4.1895	1.571013	0.402121	P ₆₁ 22	I
160	4.0992	1.568875	0.3899782	P ₆₁ 22	I
170	3.9935	1.562581	0.3584516	P ₆₁ 22	I
180	3.8947	1.556153	0.3523557	P ₆₁ 22	III*
190	3.7827	1.536208	0.295101	P ₆₁ 22	IV
200	3.7258	1.534587	0.3058081	P ₆₁ 22	III
210	3.6255	1.518815	0.2798709	P ₆₁ 22	III
220	3.5560	1.516970	0.2702824	P ₆₁ 22	III
250	3.3657	1.512323	0.267668	P ₆₁ 22	III
180a	3.8671	1.543891	0.3188191	648 P ₆₁ 22	I
180	3.8718	1.54544		648 P ₆₁ 22	I
200	3.3657	1.5024375	0.2883576	648 P ₆₁ 22	GxGyGz
220				648 P ₆₁ 22	GxGyGz
075	5.5675	1.596835	0.4742624	Pbcn	I
100	4.9652	1.589387	0.4523625	Pbcn	I
120	4.6145	1.582851	0.4385514	Pbcn	I
140	4.3276	1.576478	0.418559	Pbcn	I
160	4.0724	1.561678	0.3615409	Pbcn	I
170	3.9885	1.556033	0.3630052	Pbcn	I
180	3.8619	1.535091	0.302474	Pbcn	I
200	3.6941	1.529361	0.264194	Pbcn	IV
210	3.6246	1.522132	0.2599856	Pbcn	IV
220	3.5605	1.519139	0.257028	Pbcn	IV BG"BG"
230	3.4960	1.516730	0.2434004	Pbcn	IV
240	3.4382	1.515042	0.2521973	Pbcn	IV
260	3.3116	1.509366	0.2279203	Pbcn	IV
280	3.2103	1.506743	0.2278928	Pbcn	IV
300	3.1251	1.504065	0.2176326	Pbcn	IV

TABLE I: Data for BLYP